CrossMark

Analysis of crystallization kinetics of cast aluminum–silicon alloy

T. Tański[1] · K. Labisz[1] · B. Krupińska[1] · M. Krupiński[1] · M. Król[1] ·
R. Maniara[2] · W. Borek[1]

Abstract Light alloys like aluminum and its alloys have excellent physical and mechanical properties for a number of applications. The use of aluminum alloys can significantly decrease the mass of automobiles without decreasing structural strength. Therefore, the reason of this work was to determine the optimal cooling rate values, to achieve good mechanical properties for protection of this aluminum cast alloy from losing their work stability, and to make it more resistant to action in hard working conditions. The carried out investigations have allow to found that changes in the cooling rate do not cause changes in the phase composition, revealing the Al_2Cu and Al_5FeSi phase especially, but only changes the morphology of $\alpha + \beta$ eutectic as well as the particle size and secondary dendrite arm spacing. As a result, the number of fine crystals in per unit volume increases, leading to a fine grain structure, which influences the recalescence temperature. The purpose of this research work is to investigate the thermo-derivative interdependencies occurred in analyzed aluminum cast alloys using Universal Metallurgical Simulator and Analyzer. For the investigation, the cast AlSi9Cu aluminum alloy was used. As a result of this research, the cooling rate influence on the structure and mechanical properties changes was investigated. The cooling rate was set in a variable range of 0.16–1.25 °C s^{-1}, where the cooling rate of 0.16 °C s^{-1} corresponds to freely cooling, without any forced air flow.

Keywords Methodology of research · Metallography · Thermo–derivative analysis · Aluminum alloys · Structure

✉ W. Borek
wojciech.borek@polsl.pl

[1] Division of Materials Processing Technology, Management and Computer Techniques in Materials Science, Institute of Engineering Materials and Biomaterials, Silesian University of Technology, Konarskiego Str 18A, 44-100 Gliwice, Poland

[2] TurboCare Poland S.A., Str. Powstańców Śląskich 85, 42-701 Lubliniec, Poland

Introduction

Among the most commonly used cast aluminum alloys are the alloys with silicon, traditionally called silumins. These alloys due to its mechanical properties, excellent castability, and corrosion resistance are primarily used in engineering and automotive industry. Cast aluminum–silicon alloys were divided into hypo-eutectic with a Si concentration from 4 to 10 mass%, near eutectic with a Si concentration of 10–13 mass%, and hyper-eutectic with a Si concentration of 17 to 26 mass%. The addition of silicon that consists of alloying elements, which are as follows: Cu (0.5–5 mass%), Mg (0.2–1.5 mass%), Ni (0.6–3 mass%), and Mn (0.2–0.5 mass%). The two-component cast aluminum–silicon alloys used in industrial practice contain silicon in a concentration close to the eutectic (10–13 mass% Si). These alloys have optimum cast properties due to eutectic crystallization at a constant temperature, which affects the good castability of the molten metal and the formation of shrinkage during the casting process. In addition, they exhibit low shrinkage during the crystallization of the casts, of approximately 1.15 %, and thus insensitivity to tears and other cast defects. The disadvantage of this group of cast aluminum–silicon alloys is pure workability and lower than expected mechanical

🖄 Springer

properties of the hypo-eutectic alloys. In their structure, irregular eutectic plates with a few original silicon precipitates occur. Eutectic morphology can be changed by reducing the concentration of silicon and thermal or chemical modification [1–9, 20–24].

Paramount types of aluminum cast alloys with silicon are ternary alloys Al–Si–Cu. The cast aluminum–silicon alloys containing copper, silicon also reveal double eutectic $\alpha + Al_2Cu$, $\alpha + \beta$, and $\alpha + $ triple eutectic $Al_2Cu + \beta$. The Al_2Cu intermetallic phase occurs at a concentration of from 0.2 to 1 mass% Cu. The maximum solubility of copper—4.8 mass% occurs in the eutectic temperature and decreases to zero at room temperature. The variable solubility of copper in aluminum allows the occurrence of precipitation hardening. Crystallization of ternary alloys, Al–Si–Cu, proceeds similar for binary alloys, after crystallization of the Al–Si eutectic and $\alpha + \beta$ at a temperature of approximately 525 °C begins to crystallize the triple eutectic $\alpha + \beta + Al_2Cu$. The addition of copper moves the eutectic point toward lower concentration of silicon [1–9, 20–24]. Copper and magnesium are incorporated into the Al–Si alloys to perform heat treatment of the casts and a precipitation hardening, thereby improving their mechanical properties. In the ternary alloys of Al–Si–Cu, magnesium concentration was found in the range from 1 to 5 mass%. Due to the silicon concentration ranging from 4 to 9 mass%, the alloys are hypo-eutectic alloy. A decrease in the silicon concentration in the ternary alloys of Al–Si–Mg and Al–Si–Cu extends the solidification temperature range while also affecting the deterioration of the casting, as it makes them a tendency to shrinkage porosity, hot cracking, and reduce castability [1–9, 20–24]. Copper and magnesium are added in order to improve their mechanical properties and fatigue after solution and artificial aging. The operation is carried out to impregnate and homogenize the structure of the solid solution enriched with magnesium, silicon, and copper and rebuild the structure formed by the silicon precipitates in the eutectic structure of the casts, because during annealing at a temperature of supersaturation, changes occur concerning the preferred β phase crystal morphology, which depends on their spheroidization. This makes it possible to obtain good plastic properties despite the increase in the casting due to the strengthening of the solid solution by α phase precipitation hardening. After solution, artificial aging at a temperature of 150–180 °C for 4–8 h is carried out, during which a supersaturated of α solid solution take place to obtain the state of equilibrium by binding Cu and Mg atoms in the stable phases Mg_2Si and Al_2Cu.

Under real conditions, crystallization of aluminum alloys is slightly different from the data presented in the Al-Si Al–Si phase equilibrium diagram, which is a binary system with eutectic and limited solubility of the components in the solid state. The reason for this deviation is mainly a much faster crystallization of the melt than the corresponding crystallization according to the equilibrium conditions. This faster crystallization has the right to change the morphology of the structure of $\alpha + \beta$ eutectic or a shift of characteristic points in the phase equilibrium diagram, due to pressure increase during the crystallization of the alloy [1–6]. Knowing the crystallization itself is crucial because of changes in the structure depending on the solidification conditions and chemical composition, which determines the mechanical and functional properties, critical to choose the right substrate for further treatment.

Change of crystallization kinetic is caused by different cooling rates and influences the crystallization overcooling grade of the α solid solution and $\alpha + \beta$ eutectic, these changes can be found in the microstructure as well as in different mechanical properties of the Al–Si–Cu aluminum cast alloys. Exact knowledge of the cooling rate influence of the sand casts on structure and temperature of the phase transformations, while non-equilibrium crystallization allows to perform an optimization of the production process. The above-mentioned premises makes it possible to state that the actually studying subject matter concerning crystallization kinetics of the Al–Si–Cu aluminum cast alloys can be considered as up to date not only because of the scientifically point of view, but also for the reason of practical application of the elaborated results [1–18].

Crystallization of the liquid alloy occurs from the liquid state to the liquidus line, that is, to the beginning of the crystallization and then crystallization of the eutectics and intermetallic phases occurs to the point where the alloy is solid—the solidus line according to the equilibrium diagrams [1–3, 9–18].

For this reason on the crystallization, curie occurs some characteristic inflection points coming from exothermic or endothermic reactions of the crystallizing phase transformations. It is hard to determine unequivocally the crystallization temperature of the phases occurred on the crystallization curve. The determination is possible using the first derivative curve of the cooling line in function of time that mines using the differential ATD curve also called derivative curve.

The general equation, describing (Table 1) the crystallization function as a derivative of the crystallization, is given as (1):

$$\frac{dT}{dt} = \frac{A}{m \cdot c_p} \cdot \alpha(t) \cdot (T - T_0) + \frac{K_K}{m \cdot c_p} \cdot \left(m \frac{dz}{dt} + z \frac{dm}{dt} \right)$$

(1)

where c_p—heat capacity, m—mass of the crystallized metal, T—temperature at time dt, T_0—environment

Table 1 Chemical composition of investigated alloy/mass%

Type of material	Chemical composition of the alloy/mass%							
	Al	Zn	Mn	Si	Mg	Fe	Cu	Ti
Aluminum alloy—AlSi9Cu	88.86	0.15	0.37	9.1	0.27	0.18	1.05	0.02

temperature, A—sampler surface, K_K—crystallization constant, and z—nucleus number.

This investigation can have practical implications, for example, in the metal casting industry, for improvement of component quality that depends mainly on better control over the production parameters. This original work also provides a better understanding of the thermal characteristics and processes occurred in the near-eutectic AlSi9Cu alloy. The achieved results can be used for liquid metal processing in science and industry and obtaining of a required alloy microstructure and properties influenced by proper production conditions.

Experimental

The investigations have been carried out on test pieces of aluminum alloy (Table 1).

For performing the thermal analysis and solidification process, the UMSA (Figs. 1, 2) device was used with low-density ceramic crucibles for improving the thermal inertia
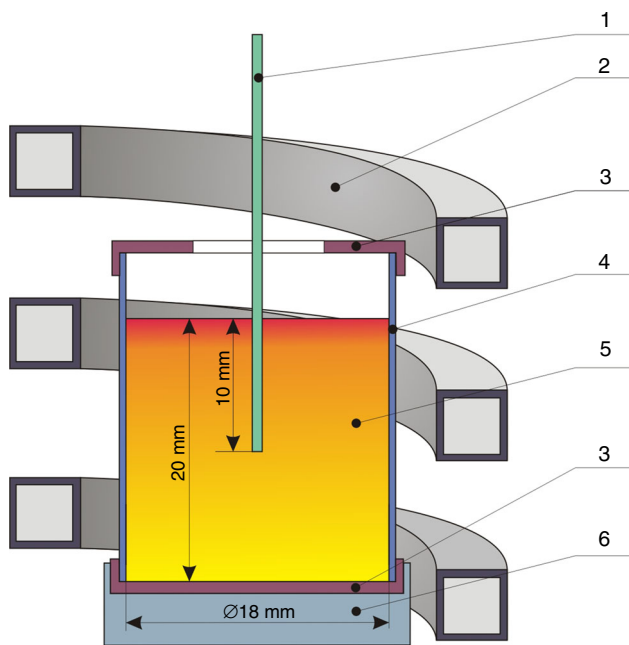

Fig. 1 Ideological scheme of the UMSA Thermal Analysis Platform experimental setup: *1* low thermal mass thermocouple, *2* heating and cooling coil, *3* thermal insulation, *4* steel foil, *5* test sample, *6* ceramic base
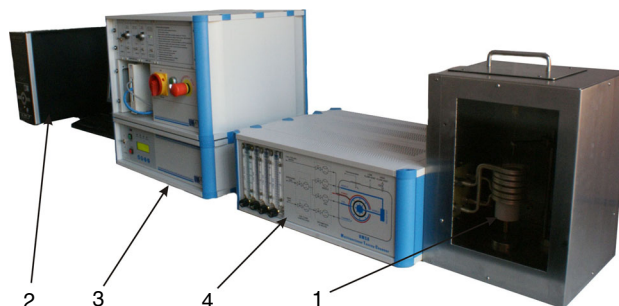

Fig. 2 UMSA apparatus, *1* sample chamber, *2* supervisory computer, *3* temperature control, *4* gas flow control

of the system. The performance of the expression thermal analysis requires a subsequent remelting, heating, and cooling of the sample with an appropriate cooling rate.

The cooling rate was calculated based on the following relationship:

$$CR = \frac{T_{ND} - T_{Sol}}{\Delta t} \tag{2}$$

where T_{ND}—nucleation temperature of the α phase dendrites, T_{Sol}—solidus temperature, and Δt—crystallization time.

Samples of circular shape with a mass of 135 g were induction-heated to a temperature of 750 ± 3 °C in graphite crucibles using the inductor (Fig. 1) powered by the generator (Fig. 2). For ensuring an appropriate cooling rate, the samples were cooled by compressed air through the nozzles placed in the inductor (Figs. 1, 2).

The intensity of the cooling airflow was controlled experimentally using the rotameter. Adequate air flow rates were determined experimentally and applied for the entire experiment. The cooling rate was set experimentally to low = 0.16 °C s^{-1} and high = 1.25 °C s^{-1}. For temperature measurement, a chromel–alumel thermocouple was applied, placed in a thermal node (determined experimentally) in the middle of the sample.

The test was repeated eight times for each cooling rate for ensuring a statistical evaluation of the obtained test results. After the registration of the cooling curve $T = f(t)$, the data were further proceeded, e.g., differential calculations and approximation for the reason to determine the differential curve. For this operation, the software OriginLab Pro 8.0 as well as the installed differential-approximate filters was used, where the approximation Savitzky–Golay filter was used.

The measurement and registration of the temperature changes in the sample $T = f(t)$ and the cooling rate of the crystallization:

$$\frac{\mathrm{d}T}{\mathrm{d}t} = f'(t) \tag{3}$$

were performed in steps dt = 0.2 s using a built-in analog–digital converter in the USMA device. After the registration of the cooling curve $T = f(t)$, the obtained data were further calculated, i.e., using differentiation and estimation for the reason of a determination of the differential curve. During the expression thermal analysis, points describing thermal processes occurring during crystallization of the alloy were determined, which have high importance for defining specific temperature and time values of the obtained expression thermal analysis curves.

For statement of the interdependence between the chemical composition and the microstructure of the AlSi9Cu aluminum cast alloy, cooled with different cooling speed, following investigations were made:

- structural studies using light microscopy MEF4A supplied by Leica together with the image analysis software, as well as structural and chemical analysis using a high-resolution scanning electron microscope ZEISS SUPRA 35 equipped with an electron gun and column of the type FEG GEMINI, detector of the in-lens type for secondary electron detections, as well as backscattered electrons detector system EDAX XM4 TRIDENT consisting of energy-dispersive spectrometer, EDS (energy-dispersive X-ray spectrometer), dedicated software, ICDD database (the International Centre for Diffraction Data); diffraction investigations and the thin foil structure investigations were performed on an transmission electron microscope JEM 3010UHR from the JEOL company with an accelerating voltage of 300 kV. The samples for optical microscope studies were etched using 0.5–2 mL hydrofluoric acid in 100 mL distilled water,
- for the reason to perform the analysis of the phase composition, the X-ray diffraction qualitative analysis of the investigated materials was performed using the XPert diffractometer supplied by Philips, by a steep recording with a steep of 0.05° and count time of 5–10 s, using filtering of the X-ray radiation $K\alpha 1$, with a wavelength of $\lambda = 1.54056$ nm coming from a lamp with copper anode,
- expression thermal analysis using the UMSA thermo-simulator (Figs. 1, 2),
- hardness was measured using the Rockwell hardness tester supplied by Zwick ZHR 4150.

Investigation results

Expression thermal analysis

During the expression thermal analysis, points describing the thermal processes occurring during crystallization of the alloy were determined, which have obtained precise signification, defining the value of the temperature and time of the thermo-derivative curves. Representative thermo-derivative curves together with selected points describe the thermal processes taking place during the crystallization, which is shown in Figs. 3, 4. Characteristic points: I, II, III, IV, V, VI, VII, VIII, which, when projected onto a cooling curve, and then the temperature axis allows to determine the temperature of phase transformation occurring during crystallization. Points describing the thermal processes taking place during the crystallization were determined using a geometric structure developed by Schultze [19]. The characteristic point of the thermal changes occurred during the crystallization process defined as the point of intersection of the tangent at the inflection point of the curve with the base curve, or as a point obtained by extrapolation of the straight sections in the expression thermal analysis (Figs. 3, 4; Table 2).

On the basis of the thermal analysis of the derivative curve, and designated as characteristic points, it was found that at the T_{DN} temperature, the nucleation process of the α phase dendrites begins, as the matrix phase, within which the next phase will be the next to crystallize. It is presented in the derivative curve as a slight inflection in point I and a temporary decrease in the cooling rate of the melt (point II). Thermal effects associated with the nucleation process provide additional heat to the remaining liquid. However, the cooling heat balance is negative. The heat supplied by the nuclei of the α phase is disproportionately smaller than the heat transferred to the environment by the cooling metal and causes only inhibition of the cooling rate of the remaining liquid. This process continues until reaching the minimum crystallization temperature of the dendritic α—phase $T_{d\min}$, wherein the nuclei are formed reaching the critical value, and where the process of crystal growth of α phase dendrites starts (section III).

A differential curve at this point is set to zero. The heat of crystallization of the remaining liquid is heated to the temperature T_{DKP}, wherein the formed and freely growing α phase dendritic crystals begin contact with each other inside some of the closing surfaces of the remaining liquid. A further crystal growth causes a temperature to increase to the maximum value of the crystallization temperature of α-phase, T_G (point IV). The chemical composition of the residual liquid varies according to the liquidus line on the

Fig. 3 Cooling curves, crystallization curves and base line of the AlSi9Cu alloy cooled with 0.16 °C s^{-1}

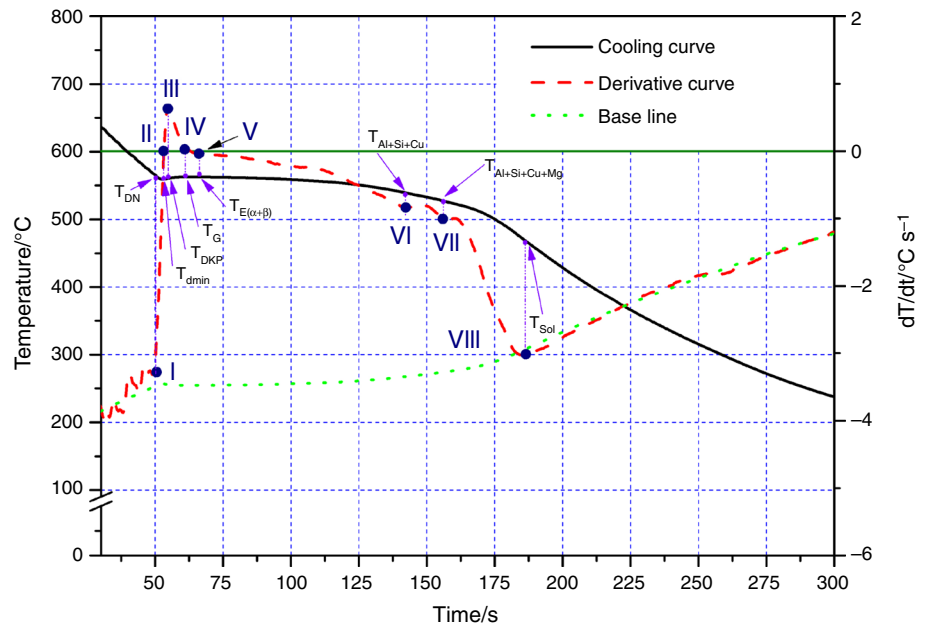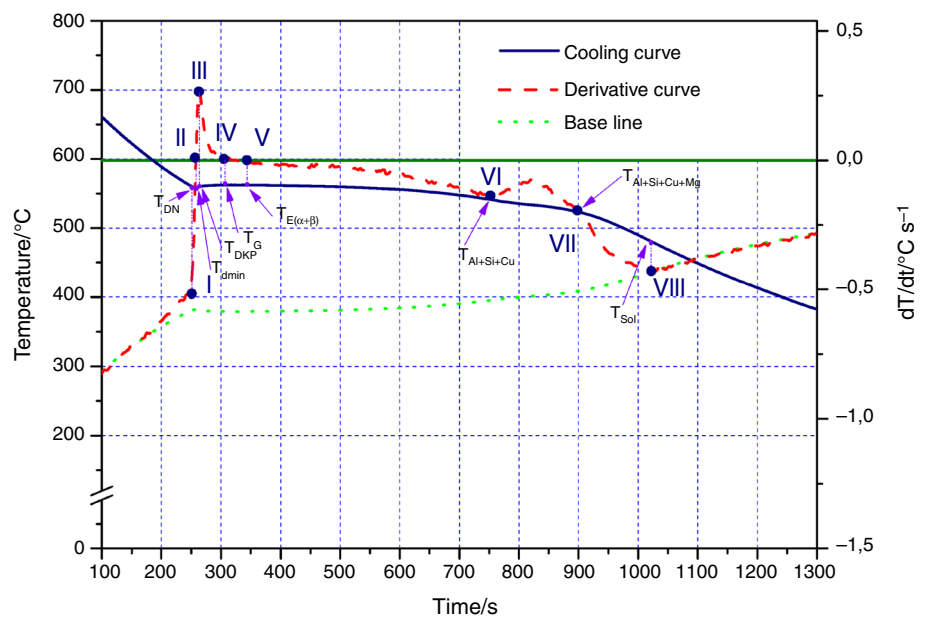**Fig. 4** Cooling curves, crystallization curves and base line of the AlSi9Cu alloy cooled with 1.25 °C s^{-1}

Al–Si diagram. The liquid is enriched with silicon, and after a temperature $T_{E(Al+Si)N}$, nucleation of $\alpha + \beta$ eutectic (point V) occurs. Upon further cooling of the remaining liquid, it is overcooled by the valued describe with the term $\Delta T_E = T_{E(Al+Si)-TE(Al+Si)min}$ and then begins the growing of the eutectic $\alpha + \beta$ (point VI). The temperature is raised to the maximum crystallization temperature of the eutectic $T_{E(Al+Si)G}$ (point VII), in which a persistent spontaneous precipitation of the α- and β-phases occurs. Further cooling the melt causes crystallization of the phase rich in copper, iron, and magnesium that produce additional crystallization heat, which is visible on the differential as apparent thermal effects (point VIII).

Based on the results of the analysis of the cooling rate of the investigated alloys, it is clear that the temperature does not significantly influence the value of α phase nucleation temperature. Increasing the cooling rate from 0.16 to 1.25 °C s^{-1} will reach the nucleation temperature of the α phase according to the line of the liquidus of the AlSi9Cu phase equal to 578 °C. As a result of measurement of the minimum and maximum crystallization temperature of the α phase, it was found that, in both studied cases, the

Table 2 Description of the characteristic points of the cooling curves presented in Fig. 3, 4

Points on the diagram	Description	Temperature/°C, cooled with	
		0.16 °C s^{-1}	1.25 °C s^{-1}
I	T_{DN} nucleation temperature. The point at which starts the nucleation of the dendrites α phase in the investigated aluminum alloys. This point is determined by the intersection of the tangent to the straight stretch of the crystallization curve to the base curve	560	561
II	T_{dmin} temperature of the begin of the crystal growth (dendrites of the α phase). Point at which the formed nuclei reach a critical value and a dendritic α phase crystal growth occurs. At this point, the first derivative of the cooling curve reaches a value zero. From this time, occurs an increase in the latent heat of the crystallization process of the dendritic α phase	557	560
III	T_{DKP} the point at which in α phase dendrites the liquid melt become a coherent. In this point, the second derivative of the cooling curve reaches a value of zero. A method of determining the point of α phase dendrite coherence is detailed described in works [2, 3, 20]	561	562
IV	T_G temperature of the end of the crystal growth (α phase dendrites). The point at which occurs a stable growth of the dendritic α phase. At this point, the derivative of the cooling curve and reaches zero similarly as at the point where occurs an increase in the latent crystallization heat. In this point, the crystallization of the Al$_5$FeSi phase occurs [25, 26]	564	563
V	$T_{E(α+β)}$ nucleation temperature of eutectic α + β. The point at which nucleation of the eutectic α + β starts. This point is determined by the intersection of the tangent drawn to the straight line of the differential curve, where the maximum cooling rate occurs after a maximum thermal effect of the crystallization of the α phase dendrite	563	564
VI	$T_{Al+Si+Cu}$ temperature of crystallization of the Al$_2$Cu phase and α + β eutectics. The point, where the crystallization of triple eutectics begins	540	539
VII	$T_{Al+Si+Cu+Mg}$ temperature of crystallization of the Mg$_2$Si phase and eutectic α + β. Point, where begins the crystallization of triple eutectics begins	523	528
VIII	T_{Sol} temperature of the end of crystallization. The point where the ends of multicomponent eutectic crystallization occur and where the alloy is fully crystallized. From this point, transformations in the solid state can only take place due to the decreasing solubility in aluminum with decreasing temperature	479	467

temperature decreases with increasing copper concentration. For the investigated alloys, where the concentration of copper is 1 mass%, it was found that there was a reduction in the minimum crystallization temperature of 476–468 °C. To generalize, it can be concluded that the increase in the cooling rate for the investigated alloys does not increase the temperature of the α phase dendrites nucleation; however, the nucleation temperature of the eutectic α + β significantly decreases the solidus temperature.

The presented characteristic points describing the thermal processes occurring during crystallization of the investigated alloys using the differential calculations determine the:

- local extreme points of the function (3)—point III; place of where the function achieves the value zero points: II, IV, V and characteristic changes of the function (3) shape points: I, III, VI, VII, VIII.

Structural analysis

As a result of the carried out investigations concerning the elements distribution using quantitative X-ray microanalysis, by appliance of EDS spectrometer, the presence of the main alloying elements Al, Si, Cu, Mg, and Fe as compounds of the cast AlSi9Cu aluminum alloy cooled with the assumed in the experiment cooling rates was confirmed (Figs. 5, 6), providing information about the mass and atomic concentration of each element in the tested places and microareas of the matrix and precipitates. Microstructural observations performed using scanning electron microscopy and quantitative EDS microanalysis, which confirms the presence of the α + β eutectic in the investigated alloys and suggest that triple eutectic like α + Al$_2$Cu + β also occurs (Fig. 5). Moreover, in the investigated alloys, multieutectics were also observed,
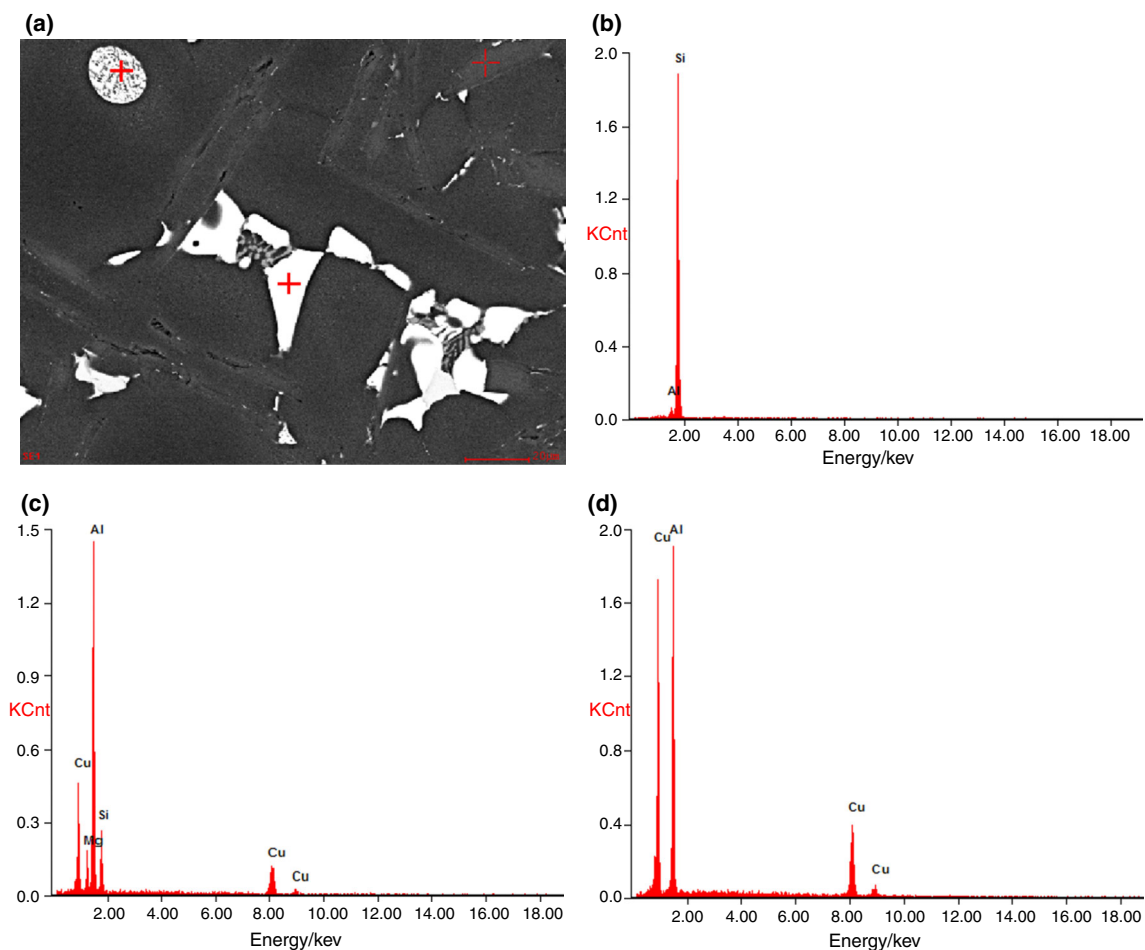
Fig. 5 a Structure of the cast aluminum alloy AlSi9Cu cooled with a rate of 0.16 °C s^{-1}; EDS pointwise analysis of the investigated aluminum cast alloy, **b** marker 1, **c** marker 2, **d** marker 3

most likely of the α + Al$_2$Cu + Mg$_2$Si + β, in which the occurrence in this group of alloys is presented in the literature [2–4, 21–24], (Figs. 5, 6).

Investigations that were carried out reveal that a significant Al$_2$Cu and Mg$_2$Si phase concentration occurs in form of conglomerates, which confirms the crystallization sequence (α + Al$_2$Cu + Mg$_2$Si + β) of the mixture of phases visible on the derivative curves (Figs. 6–10). It was state, as a result of thin foil investigation on transmission electron microscope, that the structure of the investigated alloys cooled with the applied cooling rates during the tests is mainly composed of Al$_2$Cu (Fig. 7) phase precipitations, with a morphology depending on chemical composition, as well on the cooling rate value. As a result of thin foil investigation on the transmission electron microscopy was confirmed the presence of the β-Si phase in the structure of cast AlSi9Cu aluminum alloys cooled with the cooling rates used in this experiment, these precipitates are distributed in the matrix, in form of large agglomerates of a lamellar or fibrous eutectic particles forming the α + β

grains (Figs. 7, 8). Moreover, the investigations of thin foils reveal the presence of non-uniformly distributed precipitates of the Al$_5$SiFe phase (Fig. 9), forming spherical conglomerates of fine precipitates having an average diameter of ∼ 15 μm. Precipitations of this phase are likely a compound and structural component of the ternary eutectic crystallizing in the final stage of the crystallization process.

In Fig. 11 are presented the X-ray diffractions of the investigated alloy, cooled with the assumed cooling rates. Using X-ray qualitative and quantitative diffraction methods, it was found that in the studied materials, the α-Al as the alloy matrix, β-Si phases as well as the Al$_2$Cu phase are present. Using the X-ray diffraction method, it was not possible to detect the other precipitates, which can indicate that the proportion of these phases in the investigated alloys is below the detection level of this method and is less than 3 %. As a result of phase and chemical composition investigations of the cast AlSi9Cu aluminum alloy, differences concerning phase composition of the investigated

Fig. 6 Area analysis of chemical elements alloy AlSi9Cu cooled with a rate of 0.16 °C s^{-1}: image of secondary electrons (A) and maps of elements' distribution
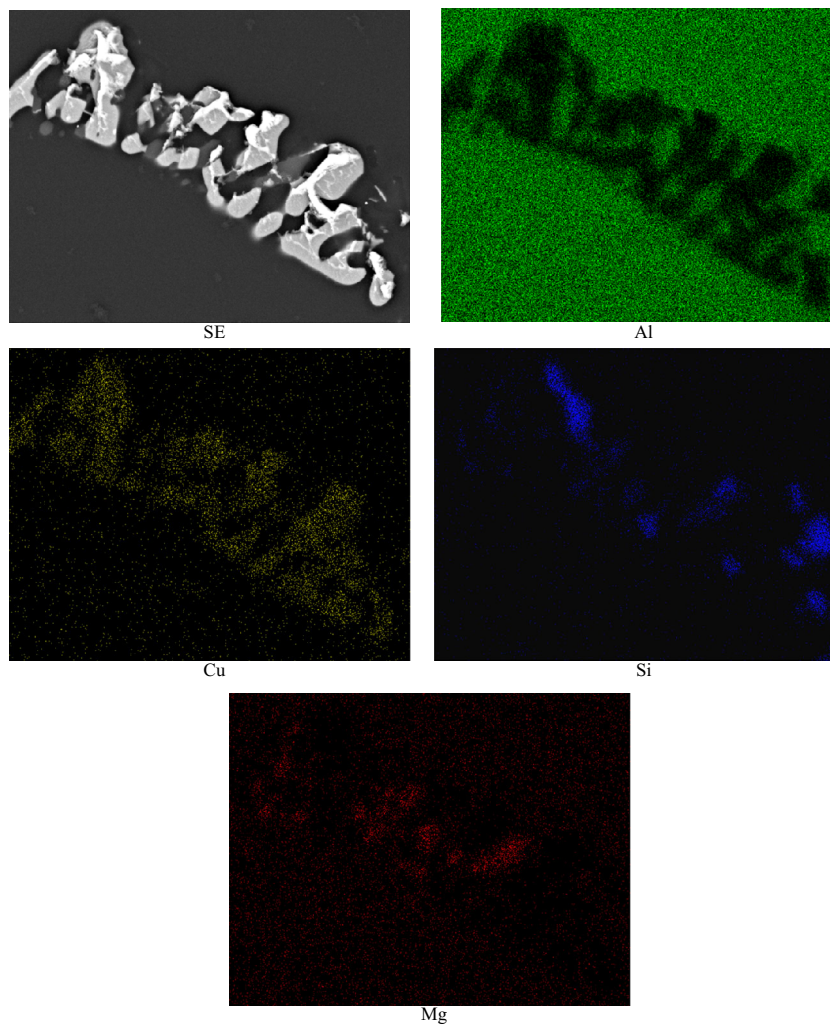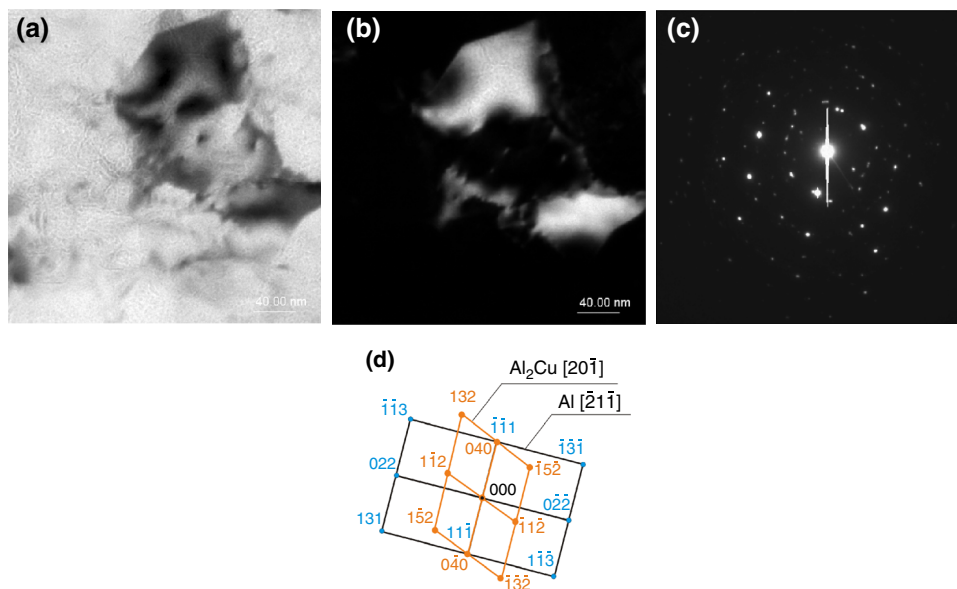

SE

Al

Cu

Si

Mg

Fig. 7 Thin foil structure from the cast aluminum alloy AlSi9Cu cooled with a rate of 0.16 °C s^{-1}: **a** bright field image of the Al$_2$Cu phase, **b** dark field image of the Al$_2$Cu phase particle, **c** diffraction pattern from the area in (**a**) and (**b**), **d** solution of the diffraction pattern from (**c**) for the Al$_2$Cu phase with zone axis [2 0 1] and the Al phase with zone axis [−2 1 1]

(a)

(b)

(c)

(d)

Al$_2$Cu [20$\bar{1}$]
Al [$\bar{2}$1$\bar{1}$]

Fig. 8 Thin foil structure from the cast aluminum alloy AlSi9Cu cooled with a rate of 0.16 °C s^{-1}: **a** bright field image of the Si phase, **b** dark field image of the Si phase, **c** diffraction pattern from the area in (**a**) and (**b**), **d** solution of the diffraction pattern from (**c**) for the Si phase with zone axis [1 0 −3]
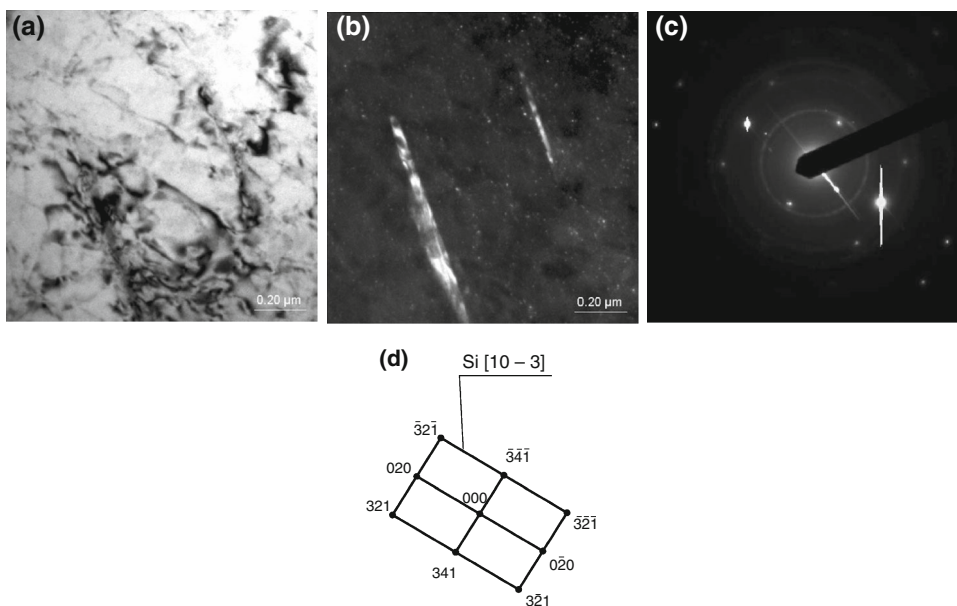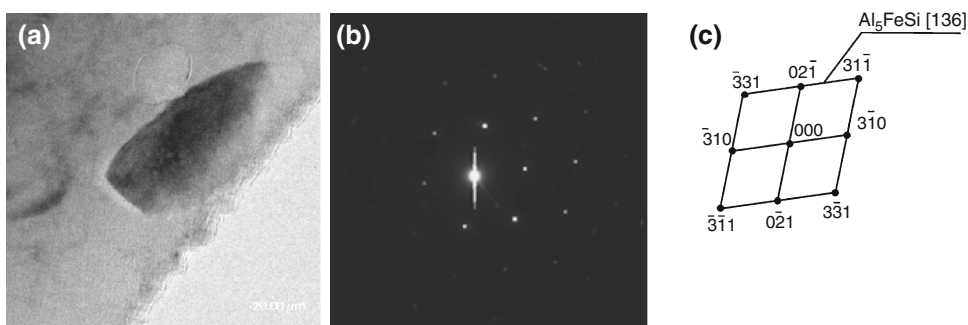

Fig. 9 Thin foil structure from the cast aluminum alloy AlSi9Cu cooled with a rate of 0.16 °C s^{-1}: **a** bright field image of the Al$_5$SiFe phase, **b** diffraction pattern from the area in (**a**), **c** solution of the diffraction pattern from (**b**) for the Al$_5$SiFe phase with zone axis [1 3 6]
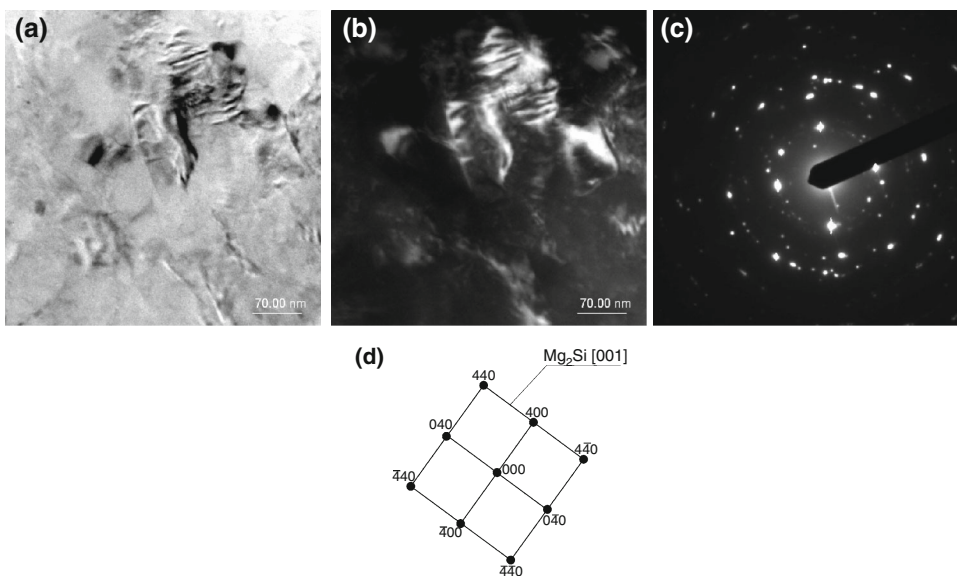

Fig. 10 Thin foil structure from the cast aluminum alloy AlSi9Cu cooled with a rate of 16 °C s^{-1}: **a** bright field image of the Mg$_2$Si phase, **b** dark field image of the Mg$_2$Si phase, **c** diffraction pattern from the area in (**a**) and (**b**), **d** solution of the diffraction pattern from (**c**) for the Mg$_2$Si phase with zone axis [0 0 1]

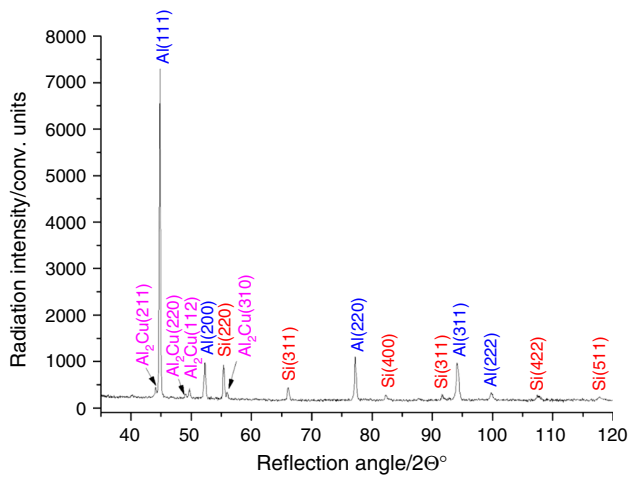**Fig. 11** X-Ray diffraction of the cast AlSi9Cu aluminum alloy slowly cooled without forced cooling 0.16 °C s^{-1}

alloys caused by different cooling rates applied to the cooled samples were not detected. Changes in the cooling rate influence the morphology of the occurring phases in the investigated alloys, especially the morphology change of the β phase.

Based on the performed investigations concerning the phase and chemical composition, as well as the literature data and presented data on the phase equilibrium diagrams, the following phase crystallization sequence of the cast AlSi9Cu aluminum alloy was determined [1–5]:
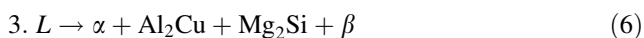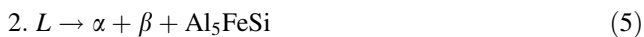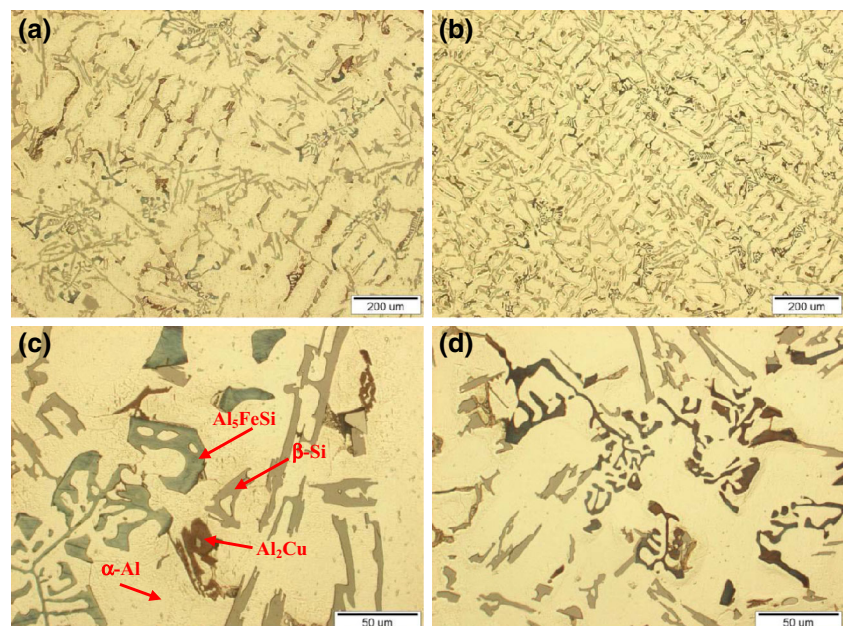
1. $L \rightarrow \mathrm{Al_{prim}}$ (4)

2. $L \rightarrow \alpha + \beta + \mathrm{Al_5FeSi}$ (5)

3. $L \rightarrow \alpha + \mathrm{Al_2Cu} + \mathrm{Mg_2Si} + \beta$ (6)

Metallographic investigation results performed on light microscope (Fig. 12) indicate that the AlSi9Cu cast aluminum alloys have a matrix structure consisting of the α solid solution and a discontinuous β-Si phase in form of grains forming the α + β eutectic. The investigated alloys are characterized by the presence of β-Si phase in form of large irregular plates with sharp corners placed in the matrix in a disordered manner, as well as with a large interfacial distance (Fig. 12). Increase in the cooling rate causes a homogenization of the structure of the investigated alloys, reduction in the interfacial distance of the α + β eutectic, and transition of a lamellar structure into needle or fiber shaped. Moreover, the structure of the investigated alloys is characterized by needle-shaped (Fig. 13a), characteristic Chinese-like characters particles (Fig. 12) of the Al$_5$FeSi phase that are generally formed near the α + Al$_2$Cu + Mg$_2$Si + β eutectics (Fig. 13b). In the investigated cast AlSi9Cu aluminum alloy, the Al$_2$Cu phase is present as a component of the triple eutectic as well as a separate colored in brown precipitation of irregular shape (Fig. 13b).

Analyzing the effect of cooling rate on the grain size, it was found that for each investigated sample, the cooling rate increase causes grain refinement and change of the secondary dendrite arm spacing. The increase in cooling rate from 0.16 to 1.25 °C s^{-1} for the investigated alloy causes more than twice a decrease in the grain size (Tables 3, 4). As the investigations reveal, the cooling rate has a crucial influence on the secondary dendrite arm spacing. This distance for the investigated alloy cooled with a rate of 0.16 °C s^{-1} is equal 79.05 μm. The increase in cooling rate to 1.25 °C s^{-1} results in a rise of the

Fig. 12 Structure of the cast AlSi9Cu aluminum alloy cooled with a cooling rate of **a, c** 0.16 °C s^{-1}, **b, d** 1.04 °C s^{-1}

Fig. 13 Structure of the cast AlSi9Cu aluminum alloy cooled with a rate of **a** 0.16 °C s^{-1}, **b** 0.48 °C s^{-1}
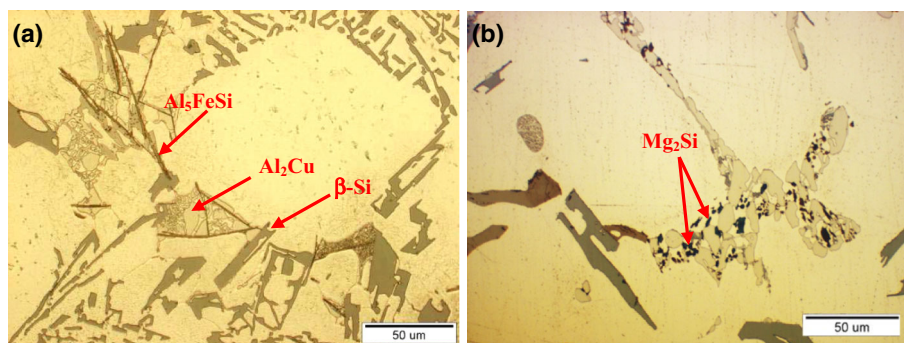

Table 3 Mean grain size, grain density, and the secondary dendrite arm spacing—λ_2, of the AlSi9Cu alloy, cooled with the cooling rate of 0.16 °C s^{-1}

Measured value	Mean value	Min.	Max.
Grain size/μm	5284.89	4162.67	5900
Grain density/10^{-7} μm^{-3}	5.76	3	9
λ_2/μm	79.05	61.03	92.52

Table 4 Mean grain size, grain density, and the secondary dendrite arm spacing—λ_2, of the AlSi9Cu alloy, cooled with the cooling rate of 1.25 °C s^{-1}

Measured value	Mean value	Min.	Max.
Grain size/μm	2111.78	1913.66	2322
Grain density/10^{-7} μm^{-3}	45.12	25	62
λ_2/μm	23.26	17.81	48.22

dendrite arms spacing more than three times to a value of 23.26 microns (Tables 3, 4).

Generally, it can be found that the increase in the cooling rate for the investigated alloys does not raise the nucleation temperature of α phase dendrites, as well as the nucleation temperature of eutectic α + β, however, significantly affect the solidus temperature reduction.

Mechanical properties such as hardness of magnesium alloys are strongly dependent on the grain size, which is, on the other hand, shown above, dependent on the cooling rate. As a result of structure changes of the investigated alloys due to changes in cooling conditions, the mechanical properties of these alloys increase. Change in the cooling rate in the range of 0.16 to 1.25 °C s^{-1} causes an increase in hardness from 69 to 95 HRF.

Conclusions

Application of the UMSA platform (Universal Metallurgical Simulator and Analyzer) allows it to determine the liquidus/solidus points of the solidified alloy directly from the cooling curve, after some calculations. Also, the points, where a phase or eutectic crystallization occurs, could be determined using this method.

In general, analyzing the effect of cooling rate influence on the grain size, it was found that for each investigated sample, the cooling rate increase causes grain refinement and change of the secondary dendrite arm spacing. The investigations reveal that the cooling rate has a crucial influence on the secondary dendrite arm spacing, as well as for the grain size. For example, the cooling rate increases from 0.16 to 1.25 °C s^{-1} two and half times a decrease in the grain size. The increase in cooling rate to 1.25 °C s^{-1} also results in a rise of the dendrite arm spacing more than three times to 23.26 microns. Changes in grains size caused an increase in the cooling rate causes by increasing the hardness of studied aluminum alloy.

The cooling rate of 0.16 °C s^{-1} was chosen, because it is the measured rate of cooling, which corresponds to freely cooling of the investigated amount of material in one sample, whereas the cooling rate of 1.25 °C s^{-1} was chosen as the maximum measurable one. Of course, in industrial processes, even higher or much higher cooling rates occur, but the presented data are obtained based on laboratory arrangement of this experiment.

The investigations performed on the cast AlSi9Cu aluminum alloy, using the metallurgical UMSA simulator with a recording equipment, allowed it to investigate the interdependencies occurred between phase morphology and cooling rate using expression thermal analysis. So the performed investigations allow to determine also the microstructure changes in a very accurate way. In general, the increase in the cooling rate causes a homogenization of the entire structure of the investigated cast AlSi9Cu aluminum alloy, reduction in the interfacial distance of the α + β eutectic, and transition of a lamellar structure into a fiber like. In the structure of the investigated alloys, the needle-like Al$_5$FeSi phase precipitates that are generally formed near the α + Al$_2$Cu + Mg$_2$Si + β eutectics are found. In the investigated cast AlSi9Cu aluminum alloy also the Al$_2$Cu phase is present in the triple eutectic.

References

1. Bäckerud L, Chai G. Solidification characteristics of aluminum alloys, vol. 3. Illinois: AFS; 1992.
2. Andberg L, Bäckerud L, Chai G, Tamminen J. Solidification characteristics of aluminum alloys, vol. 3. Illinois: AFS; 1996.
3. Bäckerud L, Król E, Tamminen J. Solidification characteristics of aluminum alloys, vol. 1. Oslo: Skanaluminum; 1986.
4. Handbook ASM. Aluminum and aluminum alloys. Ohio: ASM International; 1993.
5. Avedesian M, Baker H, editors. ASM specialty handbook: aluminum and aluminum alloys. USA: ASM International, The Materials Information Society; 1999.
6. Wróbel T, Szajnar J. Modification of pure Al and AlSi$_2$ alloy primary structure with use of electromagnetic stirring method. Arch Metall Mater. 2013;58(3):941–4.
7. Dobrzański LA, Tański T. Influence of aluminum content on behaviour of magnesium cast alloys in bentonite sand mould. Solid State Phenom. 2009;147–149:764–9.
8. Pietrowski S. Silumins. Łódź: Publisher Technical University of Łódź; 2001. p. 320.
9. Dobrzański LA, Krupiński M, Labisz K, Krupińska B, Grajcar A. Phases and structure characteristics of the near eutectic Al–Si–Cu alloy using derivative thermo analysis. Mater Sci Forum. 2010;638–642:475–80.
10. Iqbal N, van Dijk NH, Offerman SE, Geerlofs N, Moret MP, Katgerman L, Kearley GJ. In situ investigation of the crystallization kinetics and the mechanism of grain refinement in aluminum alloys. Mater Sci Eng A Struct. 2006;416(1–2):18–32.
11. Dobrzański LA, Tomiczek B, Pawlyta M, Król M. Aluminium AlMg1SiCu matrix composite materials reinforced with halloysite particles. Arch Metall Mater. 2014;59(1):333–6.
12. Chen SP, Kuijpers NC, van der Zwaag S. Effect of microsegregation and dislocations on the nucleation kinetics of precipitation in aluminum alloy AA3003. Mater Sci Eng A Struct. 2003;341(1–2):296–306.
13. Kasprzak W, Sahoo M, Sokolowski J, Yamagata H, Kurita H, Shizuoka I. The effect of the melt temperature and the cooling rate on the microstructure of the Al–20 % Si alloy used for monolithic engine blocks. Copyright 2009 American Foundry Society, International Journal of Metal Casting/Summer 09, pp 55–69.
14. Krupiński M, Krupińska B, Labisz K, Rdzawski Z, Borek W. Influence of cooling rate on crystallization kinetics on the microstructure of cast zinc alloys. J Therm Anal Calorim. 2014;118(2):1361–7.
15. Dedavid BA, Costa EM, Ferreira CRF. A study of precipitates formation in a 380.0 aluminum alloys modified by the addition of magnesium. J Therm Anal Calorim. 2002;67:473–80.
16. Farkas M, Kovács-Treer M, Závodi E. Application of DTA for controlling the heat treatment of E AlMgSi alloys. J Therm Anal. 1977;11:241–7.
17. Farahany S, Ourdjini A, Idris MH. The usage of computer-aided cooling curve thermal analysis to optimise eutectic refiner and modifier in Al–Si alloys. J Therm Anal Calorim. 2012;109:105–11.
18. Ciach R, Podosek M. Phase transformations in Al–Zn alloys solidifying at various rates. J Therm Anal. 1992;38:2077–85.
19. Schultze D. Thermo differentia analysis. Warszawa: PWN; 1974 **(in Polish)**.
20. Władysiak R. Evaluation using the thermo-derivative method (ATD) of the crystallisation, structure and properties of the Al–Si alloys with the addition of Mg, Cu, Ni, Fe modified with Sr, P, Ti, B. Not published PhD thesis, Politechnika Łódzka, Łódź, 1996 **(in Polish)**.
21. Djurdjevic MB, Kierkus WT, Sokolowski JH. Analysis of the solidification path of the 3XX family of aluminum alloys. Technical Report submitted to the NEMAK Canada Corporation, Windsor, October 2002.
22. MacKay R. Development of a new-durable Al–Si alloy for the next generation of the engine block casting. PhD thesis, University of Windsor, 2003.
23. Poniewierski Z. Crystallization of structure and properties of silumins. Warszawa: WNT; 1989 **(in Polish)**.
24. Tomiczek B, Kujawa M, Matula G, Kremzer M, Tański T, Dobrzański LA. Aluminium AlSi$_{12}$ alloy matrix composites reinforced by mullite porous preforms. Mater Sci Eng Tech. 2015;46(4):1–9.
25. Raghavan V. Al–Fe–Mn–Si (Aluminum–Iron–Manganese–Silicon). J Phase Equilib Diffus. 2007;28(2):215–7.
26. Tillová E, Chalupová M, Hurtalová L. Evolution of phases in a recycled Al–Si Cast alloy during solution treatment. Phys Scanning Electron Microscopy 2012; 411–438.